# Device modelling and model verification for the Euclid CCD273 detector

## Conference or Workshop Item

# Device Modelling and Model Verification for the Euclid CCD273 Detector

A. Clarke*[a], D. Hall[a], N. Murray[a], A. Holland[a], D.Burt[b]
[a]e2v Centre for Electronic Imaging, Dept. Physical Sciences, The Open University, England;
[b]e2v Technologies Plc. Chelmsford, England.

## ABSTRACT

Euclid is one of the M-class missions selected for the next phase of ESA's long-term Cosmic Vision programme. The primary goal of this mission is to observe the distribution and shapes of distant galaxies, with the aim of mapping and characterising the dark energy which makes up about 70% of the universe. This will be achieved by measuring the effects of weak lensing on the captured images, in terms of the distortion caused to the elipticity of galaxy shapes [1].

The e2v CCD273 was designed for the Euclid mission and is adapted from an older design (the CCD203) with changes made to improve CTE under irradiation by solar protons. Reducing the effects of radiation damage in the image sensor will result in images which have minimal distortion.

This paper is focused on the on-going development and verification of 3D device models and their integration with Monte Carlo radiation damage models. Parameters such as charge interaction volume versus signal size, pixel full well capacity, and charge transfer behaviour for both the parallel and serial registers will be discussed.

The main mission goals are aimed at measuring distortion due to weak lensing, so it is important to differentiate this from distortion due to radiation damage. This work will eventually lead to a method of post processing images to remove the effects of radiation damage.

**Keywords:** CCD, Radiation Damage, Euclid, Device Modelling, CTE.

## 1. INTRODUCTION

Euclid is a future ESA mission, which is part of the longer term Cosmic Vision programme [2]. Its primary aim is to conduct a large, detailed survey of the distribution and shape of distant galaxies over 15000 $deg^2$ of extra galactic sky [3]. This will enable astronomers to map the distribution of dark matter throughout the visible universe by conducting a weak lensing survey [1], which requires accurate and detailed images of large numbers of distant galaxies. Statistical analysis can then be used to measure the very slight distortions to galaxy shapes and positions caused by weak lensing.

A major disadvantage of using a CCD in a radiation environment is the need to transfer charge from pixel to pixel during readout. This is not usually a problem because the Charge Transfer Efficiency (CTE) in scientific CCDs is very close to 100%. However, irradiation by solar protons in the space environment can cause damage to the CCDs, reducing CTE and causing distortion to the captured images [4].

The CCD273 image sensor has been designed by e2v technologies (UK) for use on the Euclid mission [5]. It has an improved design for performance under irradiation compared to its predecessor, the CCD203. This paper documents the device modelling used to predict device parameters and explore charge distribution in the device structure, which is essential to understanding and accurately predicting charge trapping effects caused by radiation damage.

## 2. RADIATION DAMAGE

Radiation damage can cause a number of defects to form in silicon devices. The defects vary according to the type of radiating particle and its energy. As Euclid will be a space telescope orbiting at L2, the main concern for this device are energetic protons expelled from the Sun.

Solar protons incident on a CCD cause traps to form by displacing silicon atoms from their lattice positions [6]. This creates an interstitial silicon atom, and a gap in the silicon lattice known as a vacancy. A large proportion of these interactions will result in the Silicon atom recombining with its vacancy, in which case there is no net effect on the device, this recombination process is known as short term annealing. However, in a few instances the vacancy will migrate away from its original position, throughout the device structure until it becomes stable.

Research has shown that a number of stable states can be achieved by the silicon vacancy, but one of the most problematic for CCDs is the Phosphorus-Vacancy (P-V) centre, also known as the E-centre, which occurs when the vacancy combines with a donor Phosphorus atom **[4]**. These commonly occur in the n-type (Phosphorous doped), buried channel region of a CCD where they form electron traps.

E-centers, along with some other defect types, act as electron sinks, trapping any electrons which come into contact with them and re-emitting them at random. This process can be described by capture and emission time constants, as described by Shockley Read Hall (SRH) Theory, which vary depending on the trap type and the temperature [6].

### 2.1 Capture and Emission

Electrons, as majority carriers in the n-type buried channel, can become temporarily trapped in a shallow energy level created by a radiation induced defect [6]. The charge trapping process can be described by Shockley-Read-Hall (SRH) Theory [6] which determines the probability of trapping based on the charge density, capture cross-section and the thermal velocity of the electrons, but ultimately depends upon the charge packet coming into contact with the defect.

The emission probability of trapped charge varies depending on the trapping defect and temperature. Generally, as charge packets loose signal carriers to traps, the CTE will decrease. However, this depends heavily on the emission time constant as defined in SRH theory and the frequency at which the device is operated.

There are many possible scenarios for capture and emission, depending on the transfer time of charge through the device and the capture and emission time constants of the specific defects. Assuming the defect has trapped charge, an emission time comparable with the pixel to pixel transfer time might capture charge from one pixel and deposit it in the next. This would produce ‘charge tails’ in the captured images which cause distortion.

The device models are used to improve knowledge of the charge packet distribution within the device and the charge density across the packet, so improvements can be made to charge trapping models.

## 3. DEVICE PARAMETERS

The devices are modelled as accurately as possible according to the design documentation, but these models do not reflect any manufacturing variation which may be present. Therefore, it is necessary to test and benchmark the Silvaco TCAD models against measurable parameters in the Euclid test devices.

CCDs complete two tasks, charge collection and charge transfer. These are both dependent upon the electric and potential field structure within the device and charge collection is limited by the Full-Well Capacity (FWC), where FWC is the amount of charge which a single pixel element can contain. Driving the device beyond its “well capacity” will result in charge spilling across barrier electrodes into adjacent potential wells, which causes blooming in images. FWC is limited by a combination of the buried channel doping, the device geometry and the voltage applied to the device electrodes.

The channel parameter ($\Phi_{ch0}$) and FWC are two closely related device parameters which have been used to confirm the accuracy of the device models, because these values are directly linked to charge storage characteristics. To understand the definition of these parameters in the device models it is necessary to understand the formation and characteristics of the potential well itself.

In a n-channel CCD, a depletion region forms due to the recombination of mobile carriers located around the junction between the n-type buried channel and the bulk p-type substrate region. This causes the formation of fixed positively charged ions in the n-type buried channel and fixed negative ions in the p-type substrate [8]. The depletion region causes a potential field to form, where the potential increases from its minimum in the substrate to its maximum within the n-type buried channel, Figure 1(a).

Applying a positive voltage to the active gate electrodes reverse biases this junction, which extends the depletion region and hence the potential well further into the substrate, as seen in Figure 1(a). This also increases the maximum potential under the active gate, so that signal charge is attracted to, and collected in, this high potential area, or "potential well". Charge is held away from the surface interface because the voltage applied to the electrode is negative with respect to the maximum channel potential ($\Phi_{ch}$).

The channel parameter ($\Phi_{ch0}$) defines the potential difference between a zero voltage applied at the gate electrode and the potential which appears in the buried channel. The maximum channel potential ($\Phi_{ch}$) will always be ~$\Phi_{ch0}$ higher than the applied gate voltage when the device is fully depleted, Figure 1(a).

### 3.1 Full Well Capacity

During charge collection, signal charge generated in the CCD substrate is attracted to the potential maximum. A section of the depletion region around the maximum channel potential ($\Phi_{ch}$) becomes un-depleted, as the charge carriers compensate the fixed ions in this area, this results in a reduction of $\Phi_{ch}$, Figure 1(b). FWC is theoretically achieved when the peak channel potential has reduced to a level which is comparable to the maximum channel potential of an adjacent off (barrier) electrode. Adding charge carriers to the potential well beyond this limit will result in the potential of the collecting phase being lower than the barrier phase, thus charge will begin to "spill" towards the higher potential (now the barrier), causing blooming. Notice that the potential maximum moves towards the surface as charge accumulates in the potential well, Figure 1(b), this creates an alternative limit to the well capacity [8].

As the potential well fills and the profile moves towards the surface the chances of charge interacting with dangling bonds at the Si-$SiO_2$ interface increases. When this interaction occurs a fundamental limit to the well capacity has been surpassed, because interaction with these bonds will significantly reduce CTE. Recent work carried out at the Center for Electronic Imaging aimed at calibrating test devices for Euclid has highlighted the need to operate the devices at a slightly higher potential than anticipated. This causes the potential profile and $\Phi_{ch}$ to shift closer to the surface making surface interaction the ultimate limit to FWC in the Euclid device, according to the Silvaco models.

Probability of surface interaction can be calculated using a simple exponential formula, based on the thermal energy of charge carriers, Equation 1.

$$P(e) = e^{\frac{-\Delta V}{\left(kT/q\right)}} \tag{1}$$

Where ΔV can be derived from the potential profile, Figure 1b, as the difference between the potential at the surface interface and the maximum channel potential ($\Phi_{ch}$), kT/q is the thermal voltage; ~26mV at room temperature.

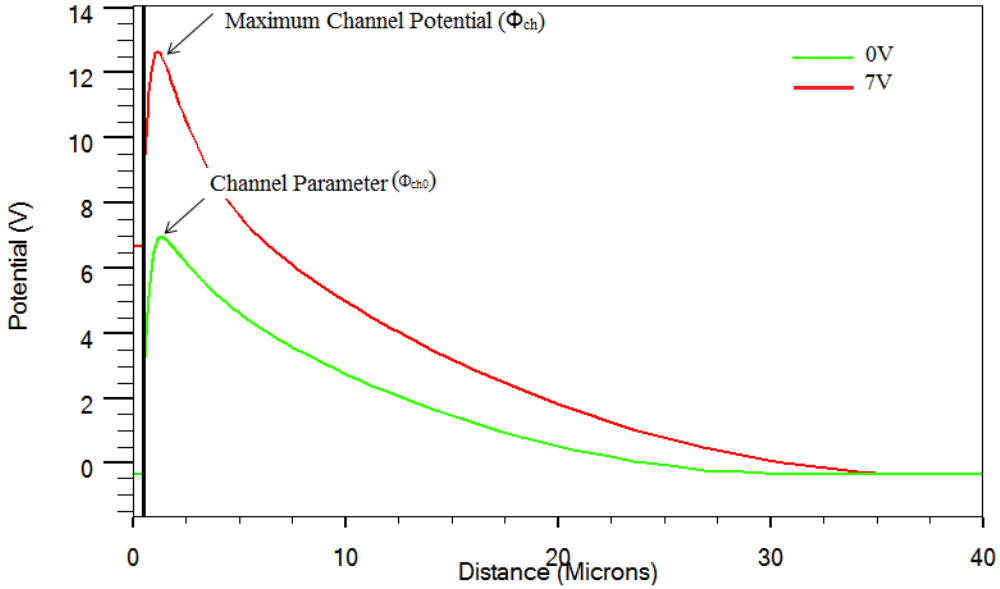


(a) The potential increases to a maximum a few microns from the surface interface (the channel parameter) and falls away to zero further into the substrate.

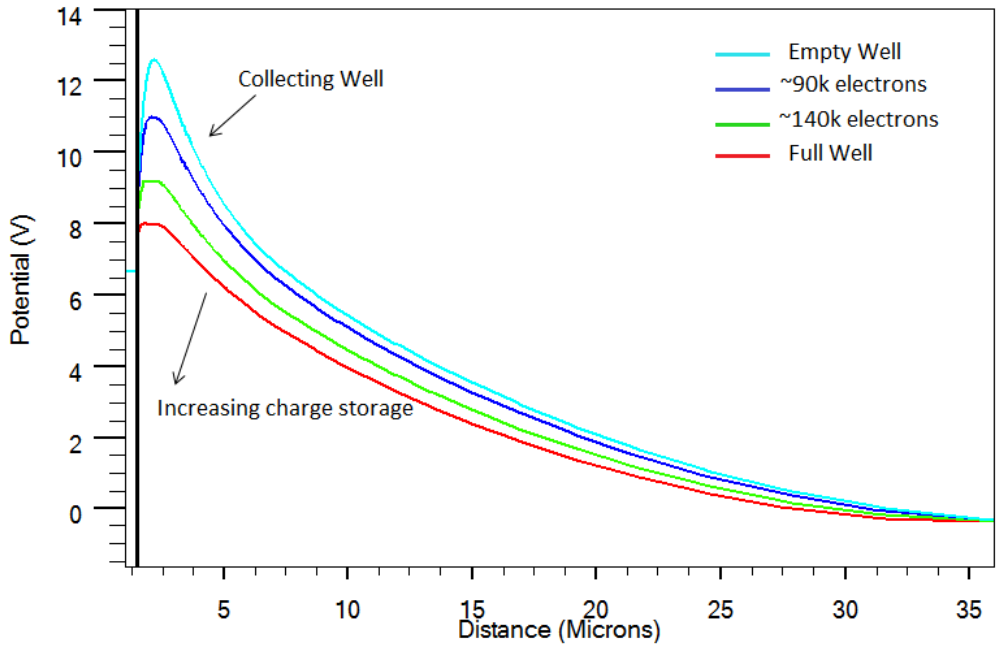


(b) A similar potential profile showing the change in the potential well under the active electrode as charge is collected.
**Figure1.** Potential profiles for the Euclid CCD as modeled using Silvaco TCAD.

With surface interaction and barrier limits in mind, the FWC has been estimated from the Silvaco models at ~220k electrons in the Euclid pixel and ~330k electrons in the register structure. This can be compared to the predicted values of 190k electrons in the pixel and 300k electrons in the register [9]. FWC has been measured for the Euclid pixel in an early test device at ~209k electrons. This is a higher value than that predicted, but very close to the FWC estimated from the models.

The channel parameter ($\Phi_{ch0}$) calculated from the Silvaco model is visible on Figure 1a at ~7V. This is almost an exact match to $\Phi_{ch0}$ measured from an early test device of ~7.1V.

## 4. CHARGE TRANSFER EFFICIENCY

Signal charge is retrieved from the CCD pixels by transferring the charge in parallel along the image area buried channel (parallel register) by sequentially clocking the gate electrodes. This occurs in stages, when each row of pixel elements is transferred to the register, they are then transferred in series until the signal from each element reaches the output node, where output from the device occurs [8]. Depending on the pixel location and the size of the device, a charge packet can undergo thousands of transfers before it reaches the output node, so it is advantageous to optimise the device CTE.

CTE is the main performance limit in radiation damaged CCDs. It is a measure of the fraction of charge which is successfully transferred from one pixel to the next during readout [8**]**. The mechanism of electron trapping, as described for radiation damage, causes CTE to degrade when the trap emission time is longer than the pixel dwell time. The later re-emission of the captured charge causes the "charge tails" visible on captured images from radiation damaged devices. Alternatively a trap with a very long emission time may only re-emit captured charge after the entire image has been read-out of the device, in which case the signal level will be reduced.

These effects are very important considerations for the Euclid device, where a charge tail caused by charge trapping can distort the PSF of a point source, such as a star, or the ellipticity of a distant galaxy. Considering the weak lensing survey, which is an integral part of the Euclid mission, will be measuring similar small distortions in the shapes of astronomical objects, it is essential that these effects can be differentiated.

Electron trapping depends upon the trap interacting with the charge packet, assuming that the proportion of the device buried channel occupied by the charge packet increases with the signal size, it is feasible that a trap close to the edge of a pixel will only trap at or near device Full Well Capacity, whereas a trap in the centre will trap both at small and high signal levels. Thus CTE can vary depending on the signal level at which CTE is measured. A more detailed description of trapping characteristics is given in [10].

Typical signal levels for the Euclid device are expected to be in the range of 90 electrons background and 200-300 electrons for the galaxies of interest. At these signal levels trap interaction would heavily depend on how charge is distributed within the device at small signal, thus device modelling to predict charge distribution is essential for understanding the trapping effects.

## 5. INTERACTION VOLUME

Traps in the CCD buried channel will only capture charge if the charge packet comes into contact with the trap. As such it is an advantage to estimate the distribution of charge in a given packet and calculate the change in charge distribution with signal size. Current trapping models assume a relationship between charge packet distribution and signal size based on the interaction volume function [11], Equation 2. This is shown graphically in Figure 2.

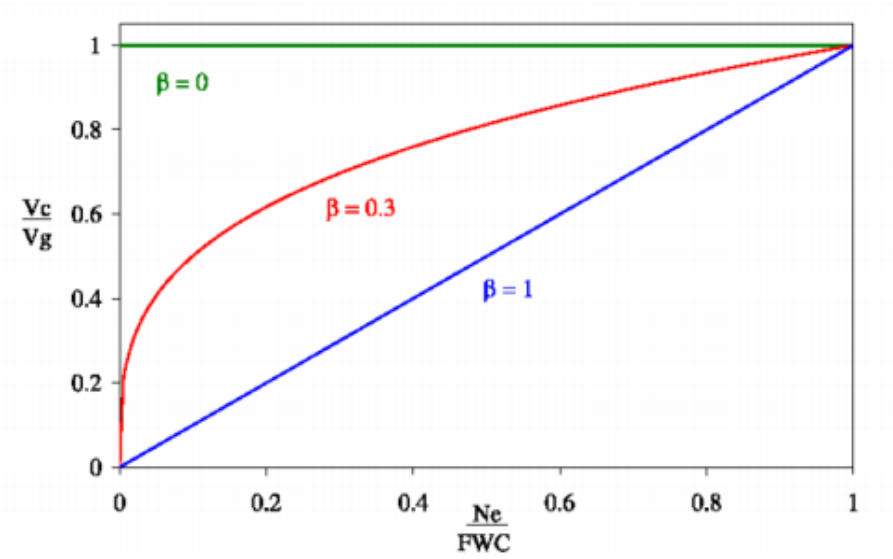


**Figure2:** Plot of the interaction volume function with varying β values to illustrate the competing charge distribution assumptions [11].

$$\frac{V_C}{V_g} = \left(\frac{N_e}{FWC}\right)^{\beta} \tag{2}$$

This function describes the change in signal-volume, with the number of electrons present. Where $V_c$ is the volume which the charge packet occupies, $V_g$ volume of the charge packet at full-well, $N_e$ is the number of electrons in the charge packet, FWC is the number of electrons at full-well and β is a fitting parameter which describes the change in signal distribution.

The interaction volume function allows several assumptions to be explored:

1. Where the fitting parameter is β=0. A charge packet of any signal size will always fill the total volume available to it. Only the charge density of the packet will change when the signal size increases.
2. Where the fitting parameter is β=1. A charge packet of any size will always have the same charge density. The volume which the charge packet occupies increases with signal level.
3. Where the fitting parameter is 0<β<1. Both the volume and density of the charge packet change with varying signal levels.

### 5.1 Interaction Volume from Device Models

Using the Silvaco models it is possible to estimate the volume of the charge packets, by observing the charge distribution in three dimensions. Measuring the modelled volume over varying signal sizes, it is possible to create a plot analogous to that of the theoretical interaction volume, Figure 3a, which is given over a log scale to accentuate the small signal characteristics, which are of interest. The charge packet distribution and hence the signal-volume model is influenced by the device doping, geometry and the applied voltages.

Difficulties arise when measuring the volume of a charge packet because the density gradually reduces towards the edges until it becomes negligible, so there is no definite edge (commonly referred to as the "fuzzy edge"). This is where the differences between the theoretical interaction volume and the physical case become apparent. Defining the volume is difficult, but it can be approximated by choosing a "cut-off density", based on charge trapping theory, where inside the defined volume, charge density is high enough to consider trapping probable [12]. Using the cut-off method to define the charge packet volume affects the calculated β parameter, which varies depending on the cut-off chosen.

Figure 3 shows data for the interaction volume calculated from the Silvaco models for both the pixel and register structures. The data ranges from a signal level ~90 electrons, which is the expected background for Euclid up to the calculated FWC, a cut-off density value of 1E12/$cm^3$ is chosen for the example data. This cut-off is equivalent to 1electron/$\mu m^3$, beyond which trapping is considered unlikely.

It is possible to modify the interaction volume function, by introducing a new variable to account for small signal deviation. This allows a better fit across the entire range of data and resembles; Volume= $\gamma S^{\beta}+\alpha$. Where α is the small signal modifier, γ is a scaling constant, S is signal size and β is the fitting parameter similar to that discussed in Section 5 [13]. This new volume model would also reduce confusion between the fitting parameter β from theory and that calculated from the Silvaco models which varies depending on the cut-off value.

Curves which offer a reasonable fit to the data are displayed in Figure 3, based on the Volume= $\gamma S^{\beta}+\alpha$ model. The change in volume differs slightly between the two structures, due to the difference in geometry. Directly comparing Figure 3a and 3b it is obvious that the register is a larger structure because the charge packet occupies a larger volume at small signal and the volume increases more rapidly as the signal level is increased.

At small signals the charge packet tends to be less dense and have a larger volume relative to the signal level. This means that the volume measured with a given cut-off becomes less reliable as the signal level reduces, but this can be improved by reducing the density of the cut-off value chosen. The cut-off value used for data in Figure 3 may not be optimal for the signal levels of interest for Euclid, but have served to improve the modelling methods.

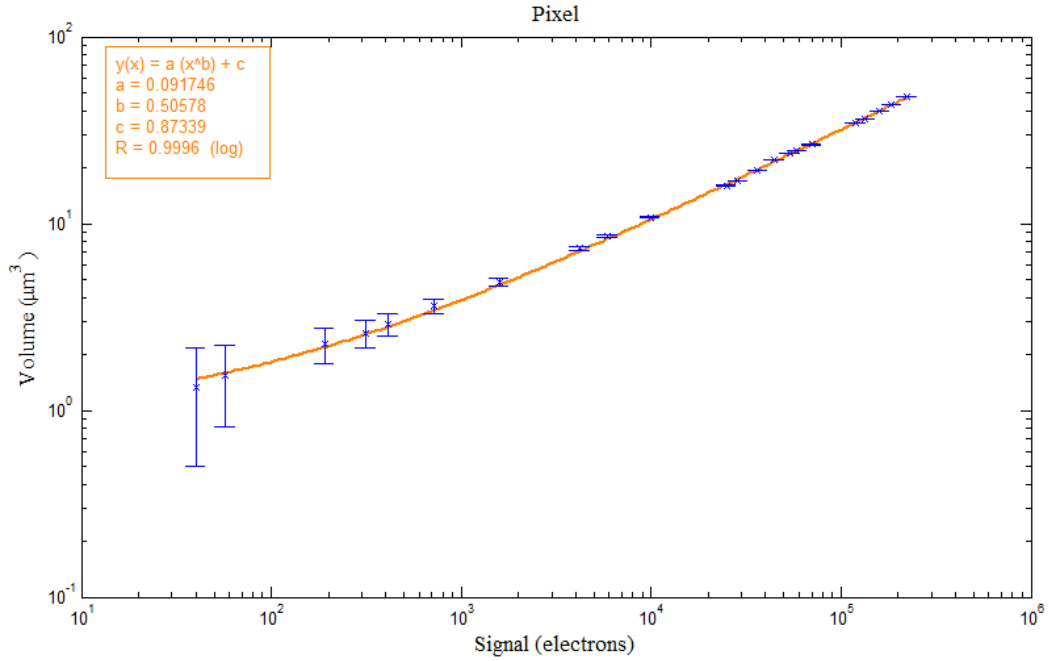


(a) Signal-Volume distribution derived from the Silvaco model for the Euclid pixel structure. The fit is given by Volume= 0.09*Signal$^{0.51}$+0.89.

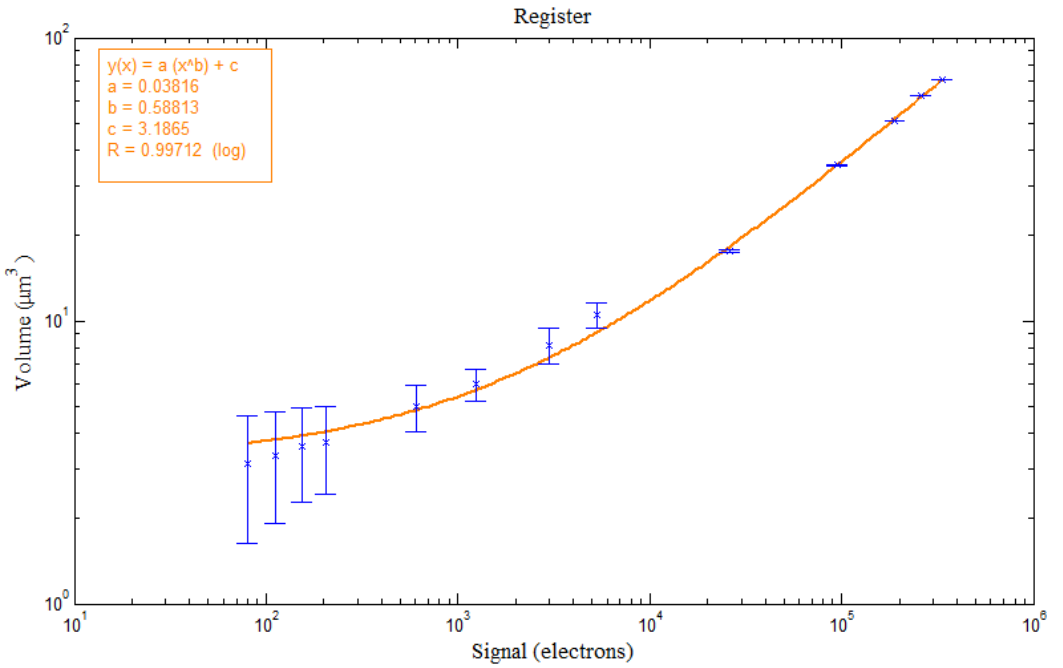


(b) Signal-Volume distribution for a Euclid Serial Register element. The fit is given by Volume=0.04*Signal$^{0.59}$+3.195.

**Figure3.** Signal-Volume distributions similar to Figure 2, derived from the Silvaco models. A fit is given based on the modified Volume= $\gamma S^{\beta}+\alpha$ equation.

### 5.2 Charge Transfer Model

An alternative approach is applied at the Open University, taking the charge distribution data directly from the Silvaco model and using it to produce a "trapping probability" distribution which is derived from the SRH equations discussed in Section 2.1[10]. These trapping probabilities can be applied directly to a Monte Carlo model to define cut-off volumes, depending on the defect position in the structure and the signal size, so that the trapping probability can be calculated more accurately.

Previous modelling efforts have included those of the CCD204, which is a radiation test chip based on the Euclid predecessor, the CCD203. A direct comparison between the models of the CCD204 and the CCD273 predicted a change in signal-volume in the serial register between 1.5x and 2x, depending on the signal level, see [12]. Recent results comparing the serial CTE of the radiation damaged CCD273 and CCD204 at the Open University have calculated a ~1.7x improvement between the two designs. These results go some way to confirming the Silvaco model accuracy and the link between signal-volume and CTE assumed in the charge transfer model.

## 6. CONCLUSIONS

This paper has outlined methods used to predict the charge distribution in CCDs using Silvaco TCAD software. Knowledge of charge distribution can give insight into the radiation performance of devices in terms of the effect of radiation damage on CTE before any device testing has been carried out; assuming CTE is directly related to the charge packet volume [12]. The modelling work improves understanding of charge collection and distribution throughout the Euclid device structures. The data generated can feed directly into charge transfer models and also offer observations for improved device operation and future device designs. The charge transfer models to which this work contributes are an integral part of the development of the Euclid mission's analysis programme.

Verifying the TCAD models against measurable parameters increases confidence in the results, because charge distribution cannot be directly observed in practice. Parameters which are directly related to charge storage, such as FWC are given priority in this respect. Methods to further verify the device models are currently being developed based on modifications to trap-pumping theory [15].

## REFERENCES


[1] Wittman, David M. et al. "Detection of Weak Gravitational Lensing Distortions of Distant Galaxies by Cosmic Dark Matter at Large Scales". arXiv:astro-ph/0003014v4 (2000).

[2] Cimatti, A. et al. "Euclid Assessment Study Report for the ESA Cosmic Visions" arXiv:0912.0914v1(2009).

[3] European Space Agency. "Euclid Definition Study Report", ESA/SRE (2011).

[4] Pickel, J et al. "Radiation Effects on Photonic Imagers- A Historical Perspective", IEEE Transactions on Nuclear Science, Vol. 50, (2003).

[5] Endicott, James et al. "Charge Coupled Devices for the ESA Euclid M-class Mission", SPIE Astronomical Telescopes and Instrumentation, 8453-3 (2012).

[6] Srour, J. R et al, "Review of Displacement Damage Effects in Silicon Devices", IEEE Transactions on Nuclear Science, (2003).

[7] Shockley, W et al, "Statistics of the Recombinations of Holes and Electrons", Physical Review. 87, (1952)

[8] Janesick, James. R [Scientific Charge Coupled Devices], SPIE Press (2001).

[9] Bowring, S. e2v technologies plc. "CCD273 Design Report", EUCV-E2V-RP-002, (2010).

[10] Hall, David. J et al. "Modelling charge transfer in a radiation damaged Charge Coupled Device for Euclid" SPIE Astronomical Telescopes and Instrumentation.8453-41 (2012).

[11] Short, Alex. "A Charge Distortion Model for Euclid", Technical Note: EUCLID_TN_ESA_AS_003_0. (2010).

[12] Clarke, Andrew. S et al, "Modelling Charge Storage in Euclid CCD Structures", Journal of Instrumentation, Vol. 7, (2012).

[13] Hall, David. J. “Euclid Monte Carlo Charge Transfer Model”, Open_Euclid_TR_09.01, (2010)
[14] Hall, David. J. “Comparison and Applicability to the Euclid Mission of the ESA CDM and the OU Monte Carlo Modelling of CCD Radiation Damage”, OPEN_EUCLID_TR-20-V1, (2011).
[15] Murray, Neil. “Mitigating Radiation Induced Charge Transfer Inefficiency in Full Frame CCD Applications by ‘Pumping Traps’, SPIE Astronomical Telescopes and Instrumentation, 8453-43, (2012).